Electronic Supplementary Information

Metal substitution as strategy for the synthesis of nonhelical heterometallic [Mo$_2$M(npo)$_4$(NCS)$_2$] string complexes (M = Fe, Co, Ni) with high single-molecule conductance

Wei-Cheng Chang,[a] Che-Wei Chang,[a] Marc Sigrist,[b] Shao-An Hua,[a] Tsai-Jung Liu,[a] Gene-Hsiang Lee,[a] Bih-Yaw Jin,*[a] Chun-hsien Chen,*[a] and Shie-Ming Peng*[ab]

[a.] Department of Chemistry and Center for Emerging Material and Advanced Devices, National Taiwan University, Taipei, Taiwan 10617
[b.] Institute of Chemistry, Academia Sinica, Taipei, Taiwan 115
E-mail: smpeng@ntu.edu.tw; chhchen@ntu.edu.tw; byjin@ntu.edu.tw

1. Synthesis of Hnpo and HMSCs 1−3 and 3'.

Preparation of 1,8-naphthyridin-2(1H)-one (Hnpo). To a cold solution of 2-amino-1,8-naphthyridine (0.01 mole in 25 mL of 2 M HCl), 25 mL of $NaNO_2(aq)$ (0.4 M) was added. The resulting mixture was stirred at room temperature for 0.5 h, after which it was poured onto ice water and neutralized with $NH_4OH(aq)$. The product was extracted with CH_2Cl_2 and purified by column chromatography on silica gel with acetone/dichloromethane (1:6) as eluent to afford a white powder. Yield: 1.17 g, 88%. ^1H NMR (400 MHz, d^6-DMSO, 25 °C): δ = 6.53 (d, J = 9.6 Hz, 1 H), 7.20−7.23 (m, 1 H), 7.89 (d, J = 9.6 Hz, 1 H), 8.07−8.10 (m, 1 H), 8.47−8.49 (m, 1 H), 12.11 (s, 1 H) ppm. MS (MALDI-TOF): m/z = 169.0 $[M + Na]^+$. IR (KBr): 3396 cm^{-1} (ν_{N-H}), 1672 cm^{-1} ($\nu_{C=O}$).

Preparation of $[Mo_2Fe(npo)_4(NCS)_2]$ (1). In a 100-mL round-bottomed flask, Hnpo (146 mg, 1 mmol), $FeCl_2$ (63 mg, 0.5 mmol), and $[Mo_2(OAc)_4]$ (129 mg, 0.3 mmol) were mixed in naphthalene (25 g). The mixture was then heated to *ca.* 220 °C and stirred at this temperature for 1.5 h. The solution was cooled to *ca.* 50 °C, and hexane (100 mL) was added before the solution was filtered. The crude material was washed with hexane (3×100 mL) to remove remaining naphthalene. CH_2Cl_2 (100 mL) was added to extract the product and NaNCS (200 mg) was added to this solution as a source of thiocyanate axial ligand. After stirring for 12 h at room temperature, the solution was filtered and washed with CH_2Cl_2 (100 mL). The crystal was formed either by layering the CH_2Cl_2 solution with hexane or by diffusion with diethyl ether. Yield: 38 mg, 16%. MS (MALDI-TOF): m/z = 885.9 $[M − NCS]^+$, 773.0 $[M − Fe(NCS)_2]^+$. IR (KBr): 1616 cm^{-1} ($\nu_{C=O}$ and/or $\nu_{C=N}$), 2036 cm^{-1} ($\nu_{C\equiv N}$), 2062 cm^{-1} ($\nu_{C\equiv N}$). EA (%): $[Mo_2Fe(npo)_4(NCS)_2]$: calcd: C 43.24, H 2.13, N 14.83; found: C 43.16, H 2.48, N 14.74.

Preparation of $[Mo_2Co(npo)_4(NCS)_2]$ (2). In a 100-mL round-bottomed flask, HMSC **1** (50 mg, 0.05 mmol) and anhydrous $CoCl_2$ (26 mg, 0.2 mmol) were mixed in naphthalene (25 g). The mixture was then heated to *ca.* 220 °C and stirred at this temperature. After 30 min, the solution was cooled to *ca.* 50 °C and hexane (100 mL) was added before filtration. The crude material was washed with hexane (3×100 mL) to remove remaining naphthalene. CH_2Cl_2 (100 mL) was added to extract the product. The crystal was formed either by layering the CH_2Cl_2 solution with hexane or by diffusion with diethyl ether. Yield: 40.7 mg, 86%. MS (MALDI-TOF): m/z = 890.9 $[M − NCS]^+$, 831.9 $[M − (NCS)_2]^+$, 773.0 $[M − Co(NCS)_2]^+$. IR (KBr): 1622 cm^{-1} ($\nu_{C=O}$ and/or $\nu_{C=N}$), 2036 cm^{-1} ($\nu_{C\equiv N}$), 2069 cm^{-1} ($\nu_{C\equiv N}$). EA (%): $[Mo_2Co(npo)_4(NCS)_2]$: calcd: C 43.10, H 2.13, N 14.78; found: C 43.18, H 2.03, N 15.07.

Preparation of $[Mo_2Ni(npo)_4(NCS)_2]$ (3). In a 100-mL round-bottomed flask, HMSC **1** (50 mg, 0.05 mmol) and $[Ni(OAc)_2 \cdot 4H_2O]$ (50 mg, 0.2 mmol) were mixed in naphthalene (25 g). The mixture was then heated to *ca.* 220 °C. After stirring at this temperature for 30 min, the solution was cooled to *ca.* 50 °C. Subsequently hexane (100 mL) was added prior to filtration of the solution. The crude material was washed with hexane (3×100 mL) to remove remaining

naphthalene.   CH$_2$Cl$_2$ (100 mL) was added to extract the product.   The crystal was formed either by layering the CH$_2$Cl$_2$ solution with hexane or by diffusion with diethyl ether.   Yield: 41.7 mg, 88%.   MS (MALDI-TOF): m/z = 889.9 [M – NCS]$^+$, 831.9 [M – (NCS)$_2$]$^+$, 773.0 [M – Ni(NCS)$_2$]$^+$.   IR (KBr): 1622 cm^{-1} ($\nu_{C=O}$ and/or), 2035 cm^{-1} ($\nu_{C\equiv N}$), 2082 cm^{-1} ($\nu_{C\equiv N}$).   EA (%): [Mo$_2$Ni(npo)$_4$(NCS)$_2$]: calcd: C 43.11, H 2.13, N 14.79; found: C 43.07, H 2.33, N 14.42.

Preparation of [Mo$_2$Ni(dpa)$_4$(NCS)$_2$] (3').   In a 100-mL round-bottomed flask, Hdpa (171 mg, 1 mmol), [Ni(OAc)$_2$·4H$_2$O] (62 mg, 0.25 mmol), and Mo$_2$(OAc)$_4$ (107 mg, 0.25 mmol) were dissolved in naphthalene (25 g).   The mixture was then heated to *ca.* 220 °C and kept at this temperature for 2 h.   NaNCS (200 mg) was added to this solution as a source of thiocyanate axial ligand.   After 30 min, this solution was cooled to *ca.* 50 °C, and hexane (100 mL) was added to this solution and then filtered.   The crude material was washed with hexane (3×100 mL) to remove naphthalene.   CH$_2$Cl$_2$ (100 mL) was added to extract the product.   The crystal was formed by layering the CH$_2$Cl$_2$ solution with hexane.   Yield: 138 mg, 53%.   MS (MALDI-TOF): m/z = 990.0 [M – NCS]$^+$, 932.0 [M – (NCS)$_2$]$^+$, 872.0 [M – Ni(NCS)$_2$]$^+$.   IR (KBr): 2018 cm^{-1} ($\nu_{N\equiv C}$), 2071 cm^{-1} ($\nu_{N\equiv C}$).   EA (%): [Mo$_2$Ni(dpa)$_4$(NCS)$_2$·(CH$_2$Cl$_2$)]: calcd: C 45.60, H 3.03, N 17.32; found: C 46.08, H 3.32, N 17.34.
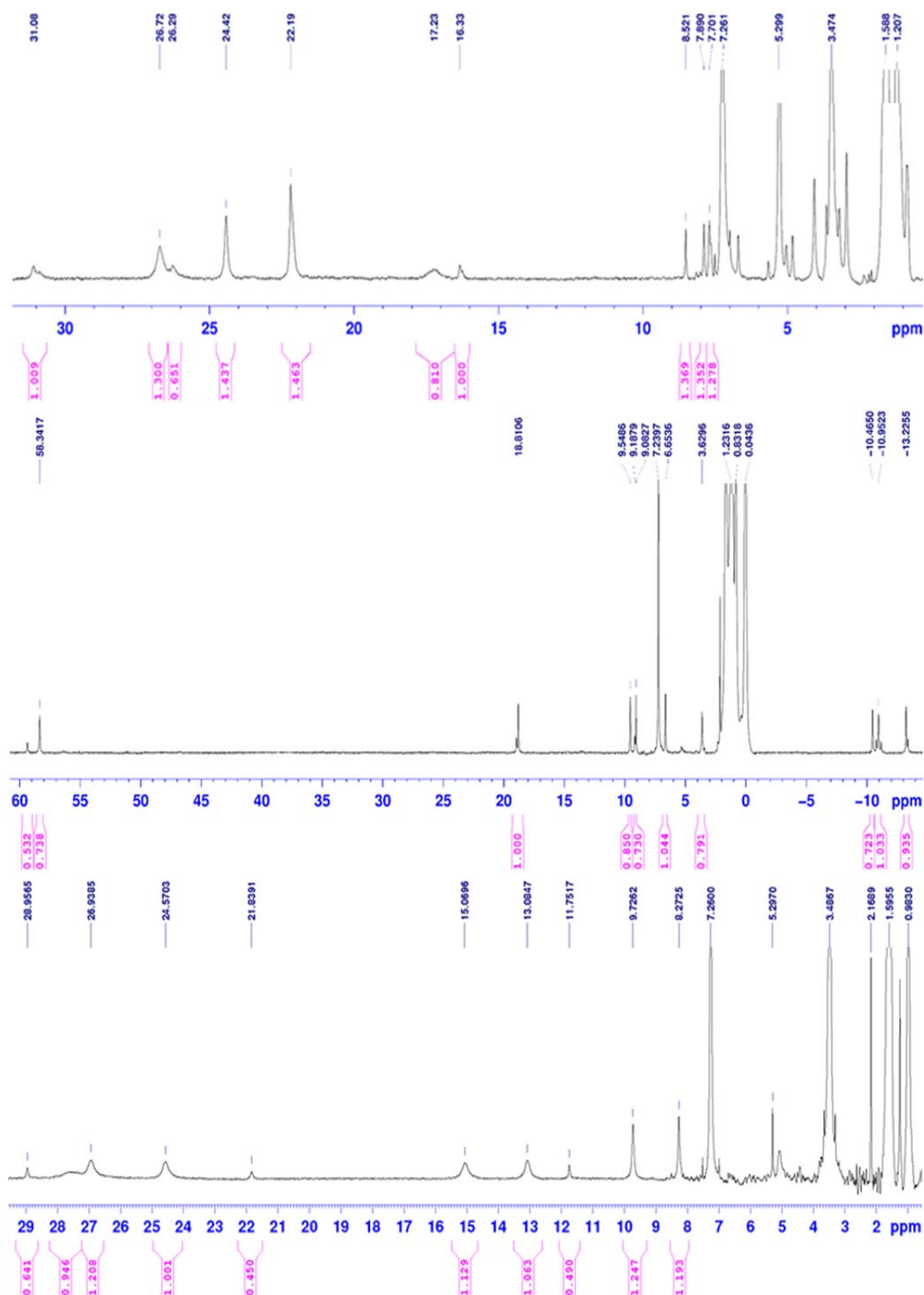
Figure S1. ^{1}H-NMR spectra of HMSCs **1** (top), **2** (middle) and **3** (bottom). Each complex exhibited 10 proton signals indicated by the pink numbers. Note that there are 5 protons in an npo$^-$ ligand. Hence, 10 proton signals implies two sets of chemical environments, consistent with the (2,2)-*trans* form determined by X-ray crystallography (see Figure S7). The presence of exactly 10 proton signals demonstrates no measurable amount of isomers or residual starting material **1** for the substituted products **2** and **3**. The solvent was CDCl$_3$ and the spectra were recorded with a Bruker AMX 400-MHz spectrometer.
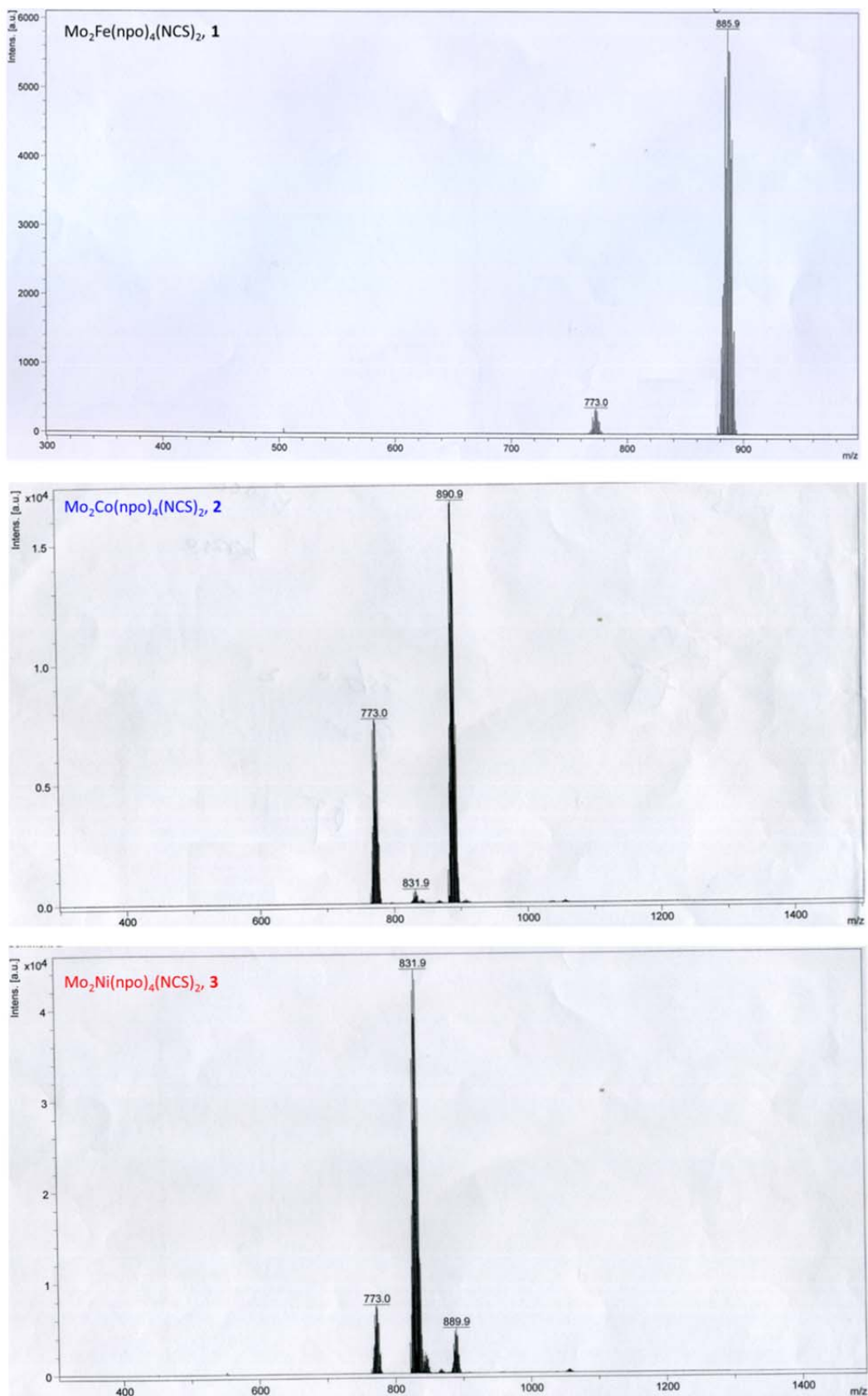
Figure S2. MALDI-TOF mass spectra of HMSCs **1−3**. $[M - NCS]^+$ fragments for **1**, **2**, and **3** are found, respectively, at 885.9, 890.9, and 889.9. The *m/z* peaks at 831.9 for **2** and **3** are ascribed to $[M - 2(NCS)]^+$ which, simulated by the natural isotope abundance, coincidentally has the same value for Co and Ni fragments. The peaks at 773.0 for **1−3** are attributed to $[M - Fe(NCS)_2]^+$, $[M - Co(NCS)_2]^+$, and $[M - Ni(NCS)_2]^+$. Mass spectra were obtained with a Bruker NEW ultrafleXtremet^{TM}.
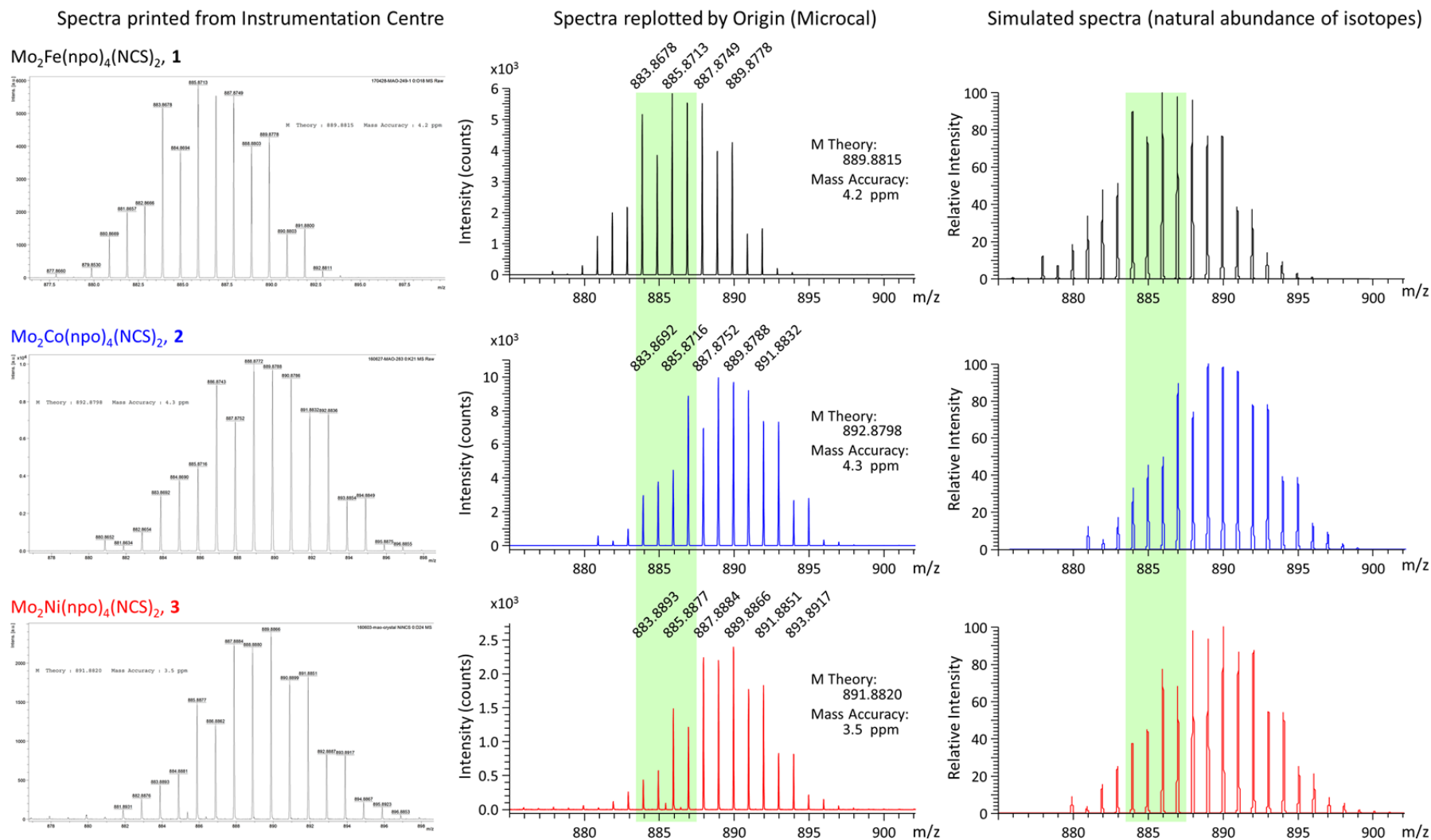
Figure S3. High-resolution mass spectra of $[M − NCS]^+$ fragment for HMSCs **1**−**3**. Left column displays the raw spectral printout with the format set by the MS facility. Middle panels are replotted spectra using larger fonts to facilitate the reading. Right panels are simulated spectra based on natural abundance of isotopes. The patterns of peak intensities agree well with measured spectra of the corresponding HMSC. The green shades highlight four strong peaks of **1**. If **1** was not removed from the studied samples of HMSCs **2** and **3** (products of displacing the Fe ion in **1** by Co and Ni, see Scheme 1 of the main text), the peak intensities in the shade should be stronger than those of the simulated ones while peaks at, *e.g.*, *ca.* 889 and 890 should be smaller. Also, the mixture would render broadened peaks for **2** and **3** because the mass digits of Fe are different than those of Co and Ni. For example, the peak at 885.8877 of **3** corresponds to 885.8713 of **1** and would be deviated from the simulated value if the sample contained **1**. The measured spectra did not show such indication and hence mass spectrometry did not observe the presence of **1** in purified HMSC **2** and **3**. Mass spectra were obtained with a Bruker NEW ultrafleXtremet™.
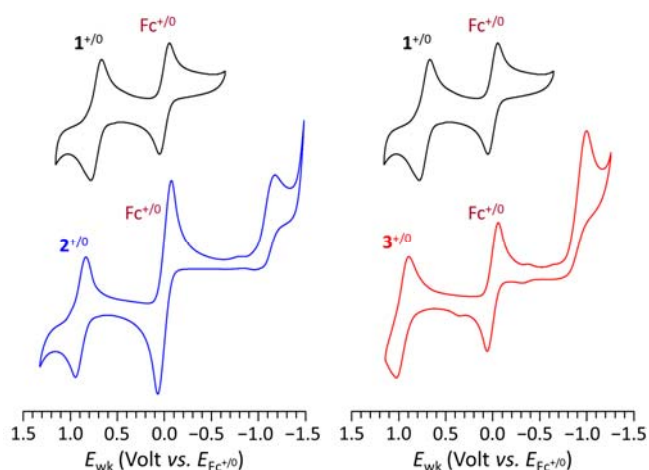
Figure S4. Cyclic voltammograms of HMSCs **1**−**3**. The values of $E_{\frac{1}{2}}$ for the first oxidation potentials of **1**, **2**, and **3** are found at 0.723 V, 0.947 V, and 0.959 V against the redox potential of ferrocene (Fc). The voltammograms of **2** and **3** appear no discernible peaks or shoulders at *ca.* 0.7 V that indicate the residue of **1**, demonstrating sufficient purification of substitution products after Fe in **1** being displaced by Co and Ni. The experiments were conducted with a potentiostat (Model 750 A, CH Instrument) under ambient conditions. Other conditions: working electrode, a 0.07-cm^2 glassy carbon disk electrode; reference electrode, a silver wire as a quasi-reference electrode; counter electrode, a platinum wire; supporting electrolyte, 0.1 M $[(Bu_4N^+)(ClO_4^-)]$; solvent, CH_2Cl_2; scan rate, 100 mV/s.
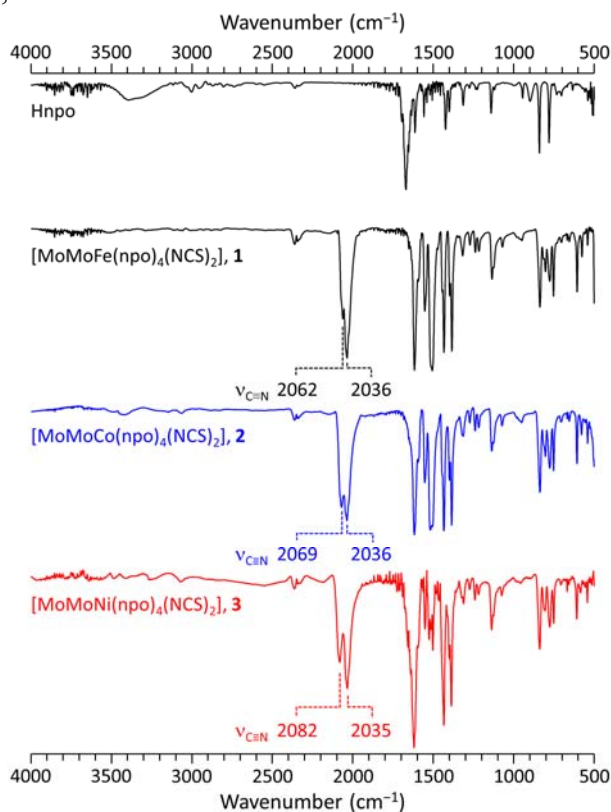
Figure S5. Infrared spectra of Hnpo (protonated ligand) and HMSCs **1**−**3**. The peaks at *ca.* 1500−1625 cm^{-1} and 2000−2090 cm^{-1} are attributed to the modes of $\nu_{C=O}$ (and $\nu_{C=N}$) and $\nu_{C\equiv N}$, respectively. The former arises from the equatorial ligand, npo. The splitting of the latter confirms the HMSC structures that the two −NCS axial ligands coordinate with different metal centres. The spectra were recorded with a Thermo Scientific Nicolet iS5 FT-IR spectrometer.
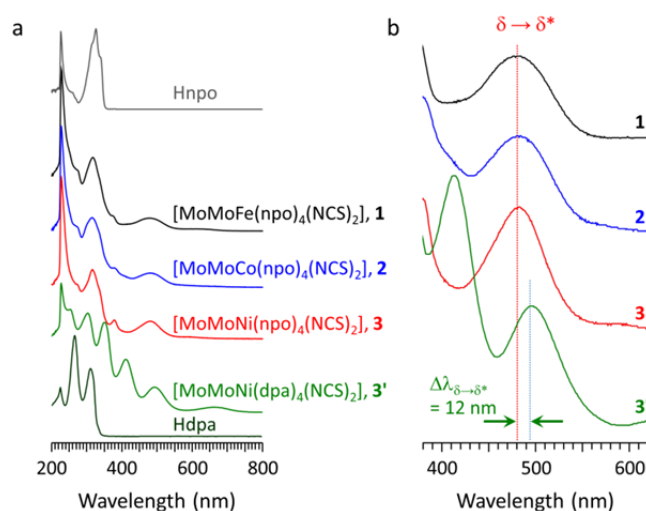
Figure S6. UV-vis spectra of HMSC **1−3** and **3'**. (a) Full spectra and (b) magnified view manifest that the δ-to-δ* transitions for **1−3** take place at 483 nm, 12 nm shorter than that of **3'** (495 nm). The difference corresponds to 62 meV or 6.0 KJ/mol, indicative of stronger δ bonds and thus larger bonding-antibonding splitting for the nonhelical HMSCs **1−3**. Spectra of Hnpo and Hdpa ligands are also displayed. For HMSC complexes, the three peaks at the short wavelengths (≤ 350 nm) are associated with the absorption of equatorial ligands. For **3'**, the peak 410 nm is attributed to ligand-to-metal charge transfer. The solvent was dichloromethane. The absorption spectra were recorded with a JASCO V-630 UV-Vis spectrophotometer.

## 2. Determination of crystallographic structures.

For HMSCs **1**−**3** and **3'**, crystallographic data were collected on a NONIUS Kappa CCD diffractometer using graphite-monochromatised Mo-Kα radiation (λ = 0.71073 Å). Cell parameters were retrieved and refined using DENZO-SMN software on all observed reflections. Data reduction was performed with the DENZO-SMN software. The empirical absorption was based on the symmetry-equivalent reflection and absorption corrections were applied using the SORTAV program. The structures were solved and refined using the SHELX programs although difficulties in the refinement of anion and solvent molecules were encountered. The hydrogen atoms were included in calculated positions and refined using a riding mode.

**Table S1.** Selected bond distances in HMSCs **1–3** and **3'**.

bond distance (Å)	**1·3CH$_2$Cl$_2$** orientation (ratio)		**2·2CH$_2$Cl$_2$** orientation (ratio)		**3·2CH$_2$Cl$_2$** orientation (ratio)		**3'·CH$_2$Cl$_2$**
	1 54.0(3) %	2 46.0(3) %	1 54.8(5) %	2 45.2(5) %	1 52.2(5) %	2 47.8(5) %	
M−NCS	2.066(8)	2.002(8)	2.088(12)	2.025(12)	2.027(10)	2.046(11)	2.032(4)
M−N(avg)	2.234(8)	2.237(8)	2.214(9)	2.218(10)	2.181(7)	2.192(8)	2.105(3)
M−O(avg)	2.078(7)	2.080(8)	2.076(8)	2.077(13)	2.068(9)	2.068(7)	-
Mo···M	2.653(9)	2.766(10)	2.635(12)	2.710(16)	2.664(10)	2.621(10)	2.546(6)
Mo≡Mo	2.151(7)	2.093(9)	2.138(9)	2.096(13)	2.057(8)	2.076(8)	2.104(5)
Mo−N$_C$(avg)	2.151(9)	2.153(11)	2.148(14)	2.150(17)	2.144(8)	2.142(9)	2.128(3)
Mo−N(avg)	2.210(6)	2.221(7)	2.202(7)	2.202(8)	2.184(7)	2.172(7)	2.199(3)
Mo−O(avg)	2.059(6)	2.062(6)	2.065(8)	2.063(7)	2.077(6)	2.064(8)	-
Mo−NCS	2.351(7)	2.356(8)	2.296(9)	2.325(12)	2.277(10)	2.284(8)	2.333(4)

The terminal metal centres of **1**, **2**, and **3** are disordered with occupancy ratios of 0.540/0.460, 0.522/0.478, and 0.452/0.548, respectively. HMSC **3'** is not disordered and, therefore, has no occupancy ratio.
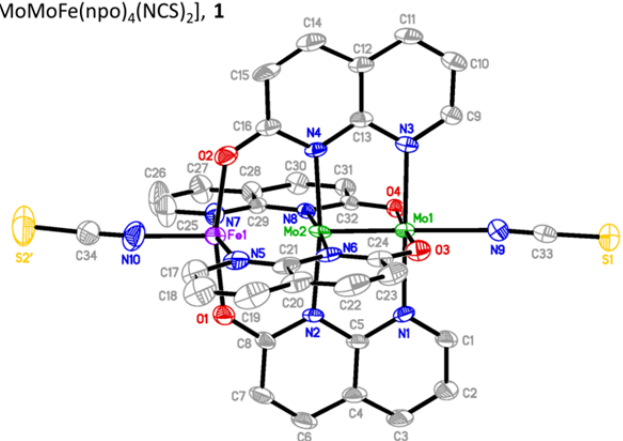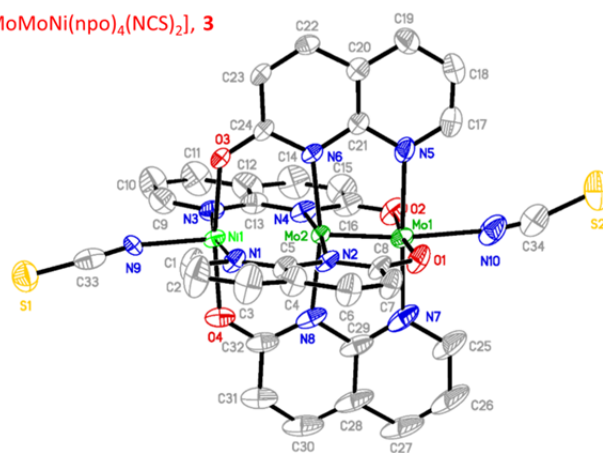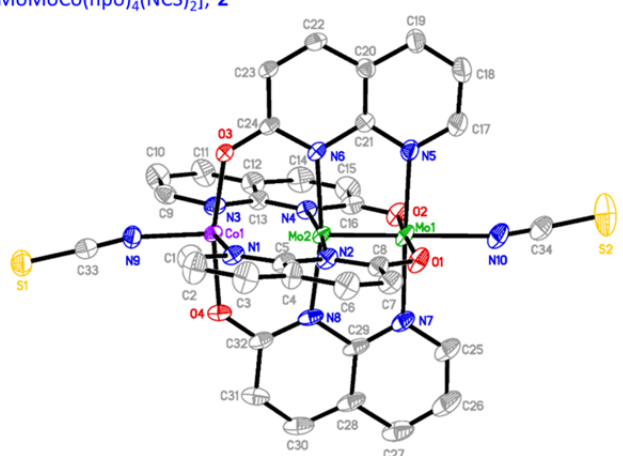
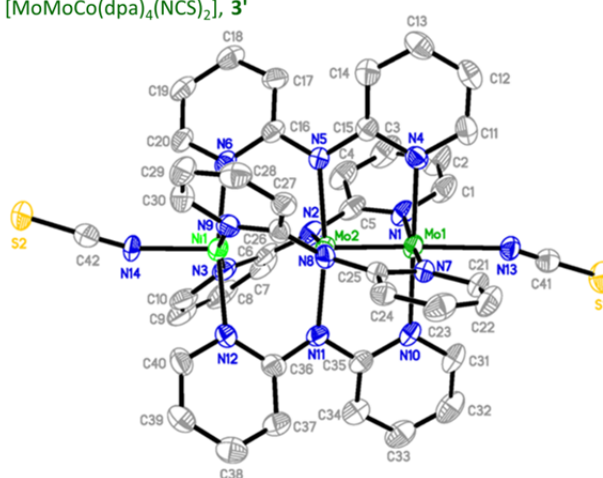**Figure S7.** ORTEP view of HMSCs **1** (50% probability), **2** (50% probability), **3** (30% probability), and **3'** (50% probability).   Hydrogen atoms and interstitial solvents are not shown for clarity.

3. SQUID measurements

Measurements of the magnetic susceptibility were carried out on a SQUID magnetometer (MPMS7, Quantum Design). Experiments of HMSCs **1**–**3** were carried out on polycrystalline samples in the temperature range of 4–300 K and a quantum external magnetic field of 3000 G. The diamagnetic corrections were evaluated from Pascal's constants. Figure S8 displays μ_{eff} values plotted against temperature.

The magnitude of spin-only magnetic moment for $[Mo_2M(npo)_4(NCS)_2]$ is estimated by $\mu_{spin-only} = [n(n + 2)]^{\frac{1}{2}}$ where n is the number of unpaired electrons of M (M = Fe, Co, and Ni) because the Mo_2 unit is diamagnetic. The numbers of unpaired electrons are $n = 4$ for **1** (Fe) and $n = 2$ for **3** (Ni) and the respective estimated $\mu_{spin-only}$ are 4.89 μ_B and 2.83 μ_B, consistent with the measured μ_{eff} of 4.96 μ_B for **1** and 3.11 μ_B for **3** at 300 K (Figure S8). However, the μ_{eff} of HMSC **2** is 4.65 μ_B, significantly larger than 3.87 μ_B for the case of 3-unpaired electrons ($= [3 \times (3 + 2)]^{\frac{1}{2}}$).

HMSC **2** was obtained by substitution of Fe atom in HMSC **1**. Hence, there is a possibility that the presence of residual **1** in the sample of **2** for SQUID measurements led to an unexpectedly high value of the magnetic moment. To have a mixture of a spin-only **2** exhibiting 4.65 μ_B would require about 70% of **1** and only 30% of **2**. Given that the ^{1}H-NMR spectrum, mass spectra, and voltammogram of HMSC **2** show no signature chemical shifts, mixed isotope patterns, and $E_{\frac{1}{2}}$ of **1**, this possibility of insufficient purification for HMSC **2** appears highly unlikely.

It is worth noting a study by Berry and co-workers[1] reporting a similarly high magnetic moment for $[Mo_2Co(dpa)_4Cl_2]$, an analogue of HMSC **2**. The magnetic susceptibility (χ) of $[Mo_2Co(dpa)_4Cl_2]$ was found with $\chi \cdot T$ of 3.00 emu·K·mol^{-1} at 300 K, equivalent to 4.90 μ_B ($\mu_{eff} = 2.828[\chi \cdot T]^{\frac{1}{2}}$). The reason why the spin-only model does not fit the magnetic moments of $[Mo_2Co(dpa)_4Cl_2]$ and HMSC **2** is ascribed to the unequal distribution of 7 d-electrons in 5 d-orbitals such that the orbital angular momentum does not quenched and results in a significant orbital contribution.[1]
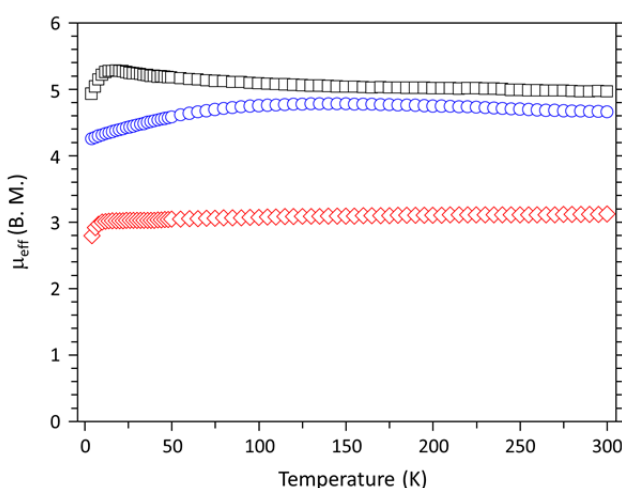
Figure S8. Temperature dependence of the magnetic moment μ_{eff} for HMSCs **1**−**3**. Black squares, $[MoMoFe(npo)_4(NCS)_2]$ (**1**); blue circles, $[MoMoCo(npo)_4(NCS)_2]$ (**2**); red diamonds, $[MoMoNi(npo)_4(NCS)_2]$ (**3**). The μ_{eff} values are temperature-independent and, therefore, indicate that HMSCs **1**−**3** are paramagnetic compounds. μ_{eff} at 300 K: **1**, 4.89 μ_B; **2**, 4.65 μ_B; **3**, 2.83 μ_B.

4. Measurements of single-molecule conductance.

Electrodes: gold STM tip and substrate.   The STM tip was a freshly cut 0.25-mm gold wire. The gold substrates were about 100-nm thick thermal deposited on a 7-nm chromium adhesive layer (99.99%, Super Conductor Materials, Inc., Suffern, NY, USA) on a piece of glass slide which were pre-cleaned with piranha solution (a 1:3 (v/v) mixture of 30% H_2O_2 and concentrated H_2SO_4). *Caution: This solution reacts violently with organics and should be handled with great care.*

Experimental procedures for STM-based break junction.   The experiments of single-molecule conductance were carried out by scanning tunnelling microscopy- based break junction (STM-BJ) with a liquid cell and a NanoScopeIIIa controller (Veeco, Santa Barbara, CA, USA).   The instrument was operated initially under the imaging mode.   If the imaging quality was stable, the imaging was interrupted and resumed after filling in propylene carbonate (PC)[1] containing saturated metal string complexes.   The operation was then switched from imaging mode to STS mode (scanning tunnelling spectroscopy) to acquire current-tip displacement traces (*i.e.*, I(s) or *i*-s traces) using a current-to-voltage amplifier with a sensitivity of 10 nA/V and recorded with a customized LabView program *via* a PXI-4461 card (National Instruments).   The STM tip was impinged onto, fused with, and pulled out of contact with the substrate (10 nm/s, 2.99 Hz) at a fixed E_{bias} 50 mV. Upon repeated formation of the tip-substrate gap, the EMAC molecules might bind across two electrodes, namely, the molecular junction.

Due to high polarity of PC, the current leakage was large and limited the measurements at the low-current regime.   Hence, the exposed area of the STM tip was reduced by coating with an insulating layer of EVA (ethylene vinyl acetate, Ted Pella, Inc.) except the apex. The details are referred to the literature listed below.[2]

For the conductance-tip displacement plots shown in Figure 2 in the main text and Figure S9, traces exhibiting purely exponential decay which apparently showed no molecule residing in between the tip-substrate junction were removed.
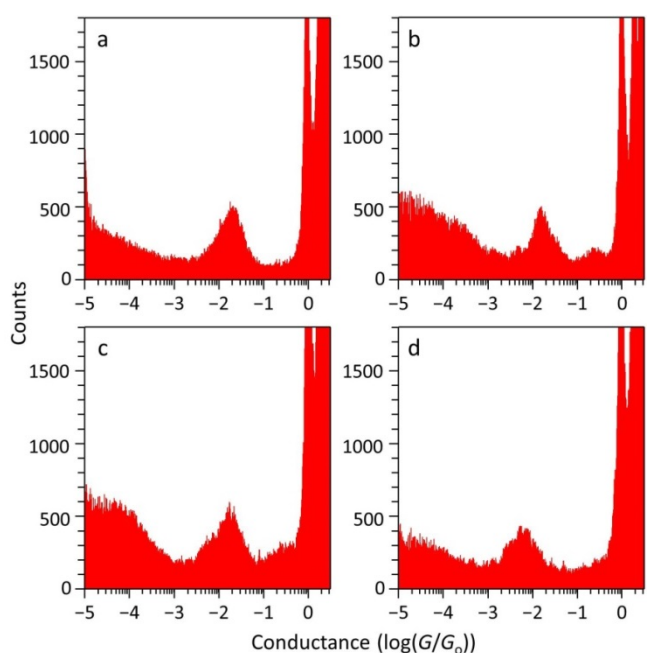

Figure S9. Conductance histograms obtained by STM BJ for (a) [MoMoFe(npo)$_4$ (NCS)$_2$] **1**, (b) [MoMoCo(npo)$_4$(NCS)$_2$] **2**, (c) [MoMoNi(npo)$_4$(NCS)$_2$] **3**, and (d) [MoMoNi(dpa)$_4$(NCS)$_2$] **3'**.   The conductance values for HMSCs **1–3** are similar and are larger (more conductive) than **3'**, manifesting the effect of the equatorial ligands.   Peak conductance: a, 20 (±12) x 10^{-3} G$_0$; b, 16 (±10) x 10^{-3} G$_0$; c, 18 (±14) x 10^{-3} G$_0$; d, 6.2 (±5.4) x 10^{-3} G$_0$.   Conditions: solution, saturated metal strings in propylene carbonate; electrodes, an EVA (ethylene vinyl acetate)-insulated gold STM tip and gold substrate; E_{bias}, 50 mV. Numbers of *G*–s traces: a, 1907; b, 1327; c, 1183; d, 1521.

5. Computational calculation:

Single point calculations were carried out using the formalism of the density functional theory (DFT) with the crystallographic results as input geometry. The split-valence basis set of Weigend and Ahlrichs[3] Def2SVP was employed because it was demonstrated good performance on EMACs calculations[4,5] on properties such as geometries and magnetism. The exchange-correlation functional is the local meta-GGA functional[6] with long-range correction[7] LC-TPSSTPSS. All calculations are carried out with Gaussian 09 package.[8] The analysis of natural bond orbitals was performed with NBO (version 3) package in Gaussian 09. The spin-corrected Mayer bond orders were taken as two times the sum of the corresponding diagonal terms from the α and β Wiberg bond index matrix. The bond order of the npo-ligated nonhelical Mo_2 unit (**3**) was found 3.10, larger than 2.80 of the prototypical HMSC **3'** coordinated by dpa$^-$ ligands.
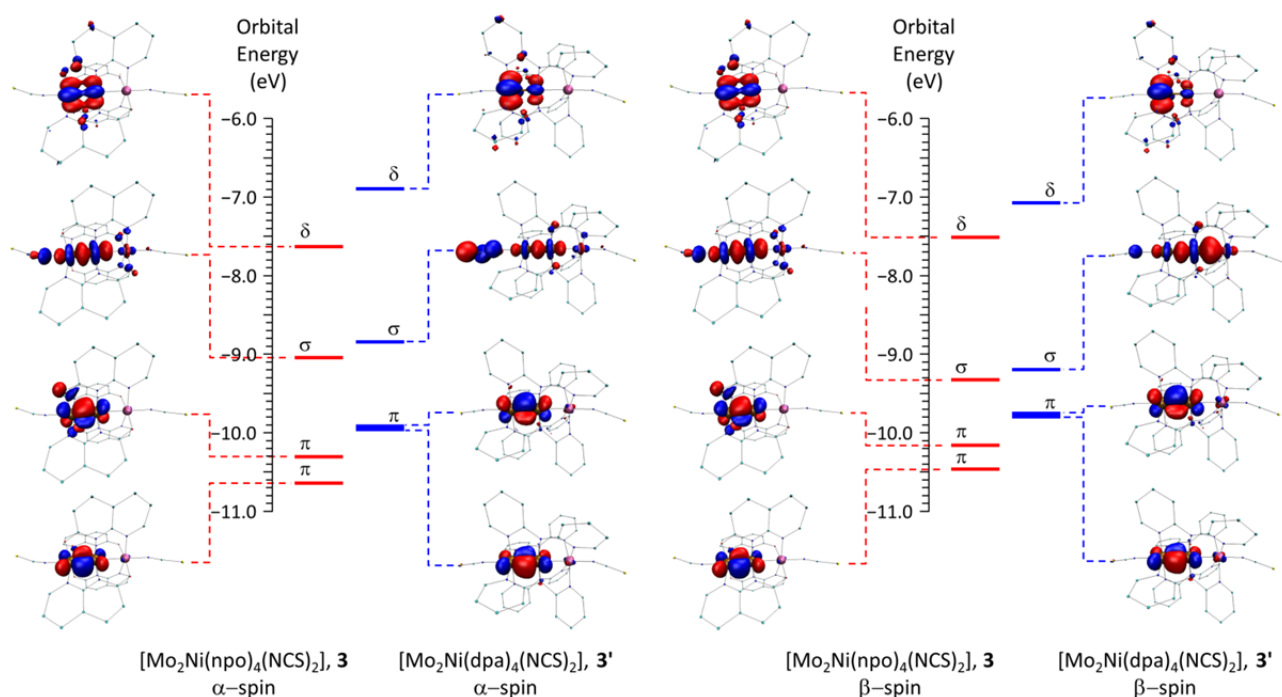
Figure S10. Comparison of molecular orbital diagrams for HMSCs **3** and **3'**. Only selected bonding orbitals associated with the metal centres are displayed. Red and blue levels represent the orbitals for [MoMoNi(npo)$_4$(NCS)$_2$] **3** and [MoMoNi(dpa)$_4$(NCS)$_2$] **3'**, respectively. δ orbitals for **3** and **3'** were found at -7.645 and -6.915 eV, respectively.
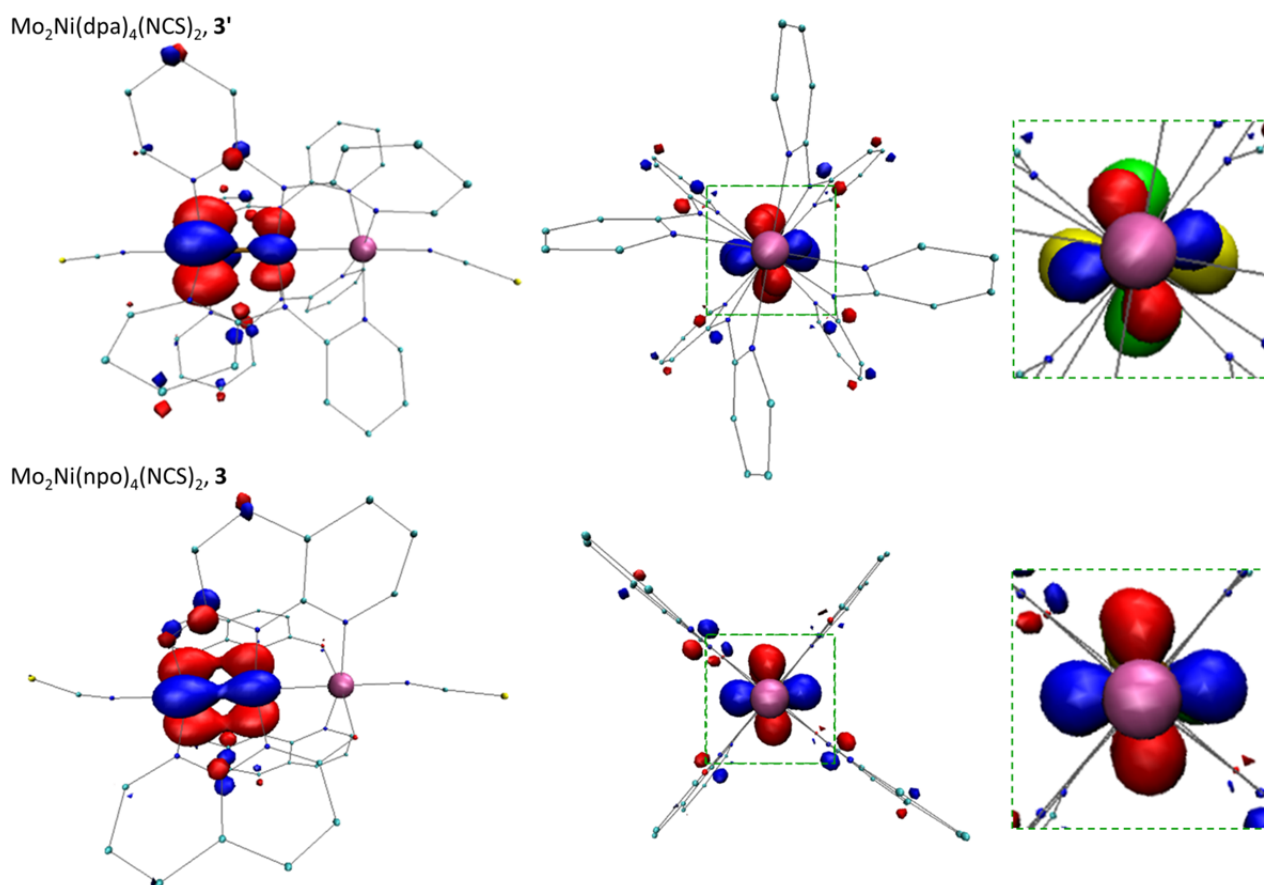
Figure S11. Results of DFT calculations on how the ligand helicity affects the δ bond orbitals of HMSCs (upper) [MoMoNi(dpa)$_4$(NCS)$_2$] and (lower row) [MoMoNi(npo)$_4$(NCS)$_2$]. The middle panels show views along the metal-metal bonds going from the Ni atom (violet-red). The helical **3'** has an apparent torsion angle between the d$_{xy}$ lobes of electron density of the two Mo atoms. To manifest the angle, the right panel presents lobes for the terminal Mo atom in green and yellow. For the nonhelical [MoMoNi(npo)$_4$(NCS)$_2$], **3**, applying the same colouring tactic confers the lower-right panel in which the torsion angle is very difficult to observe.
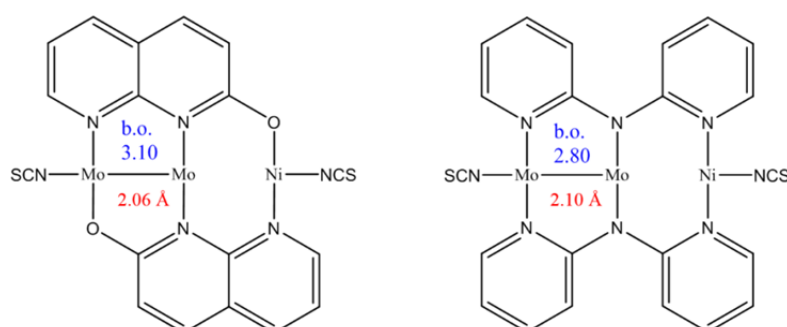
Figure S12. Scheme presentation of DFT calculations on bond orders of HMSCs **3** and **3'**. The Mo-Mo bond order in nonhelical [Mo$_2$Ni(npo)$_4$(SCN)$_2$] (**left**) is 3.10, larger than 2.80 of the helical [Mo$_2$Ni(dpa)$_4$(SCN)$_2$] (**right**). The bond lengths are in a good agreement with the crystallographic data (Table S2) of 2.057(8) and 2.076(8) Å for **3** and 2.104(5) Å for **3'**. For clarity, only two of the four equatorial ligands are drawn and the illustration at left does not imply possible conformations of [Mo$_2$Ni(npo)$_4$(SCN)$_2$] which adapts the (2,2)-*trans* form as the ORTEP view shown in Figure S7.

Reference:

1. M. Nippe, E. Victor and J. F. Berry, *Eur. J. Inorg. Chem.*, 2008, **2008**, 5569-5572.

2. T.-C. Ting, L.-Y. Hsu, M.-J. Huang, E.-C. Horng, H.-C. Lu, C.-H. Hsu, C.-H. Jiang, B.-Y. Jin, S.-M. Peng and C.-h. Chen, *Angew. Chem. Int. Ed.*, 2015, **54**, 15734-15738.

3. F. Weigend, R. Ahlrichs, *Phys. Chem. Chem. Phys.*, **2005**, *7*, 3297–3305.

4. P. Szarek, W. Grochala, *J. Phys. Chem. A*, **2015**, *119*, 35, 9363–9372.

5. P. Szarek, W. Wegner, W. Grochala, *J. Mol. Model.*, **2016**, *22*, 63.

6. J.-M. Tao, J.-P. Perdew, V.-N. Staroverov, G.-E. Scuseria, *Phys. Rev. Lett.*, **2003** *91*,146401.

7. H. Iikura, T. Tsuneda, T. Yanai, K. Hirao, *J. Chem. Phys.*, **2001**, *115*, 3540–3544.

8. M.-J. Frisch, G.-W. Trucks, H.-B. Schlegel, G.-E. Scuseria, M.-A. Robb, J.-R. Cheeseman, G. Scalmani, V. Barone, B. Mennucci, G.-A. Petersson, H. Nakatsuji, M. Caricato, X. Li, H.-P. Hratchian, A.-F. Izmaylov, J. Bloino, G. Zheng, J.-L. Sonnenberg, M. Hada, M. Ehara, K. Toyota, R. Fukuda, J. Hasegawa, M. Ishida, T. Nakajima, Y. Honda, O. Kitao, H. Nakai, T. Vreven, J.-A. Montgomery, Jr., J.-E. Peralta, F. Ogliaro, M. Bearpark, J.-J. Heyd, E. Brothers, K. N. Kudin, V. N. Staroverov, R. Kobayashi, J. Normand, K. Raghavachari, A. Rendell, J. C. Burant, S. S. Iyengar, J. Tomasi, M. Cossi, N. Rega, J. M. Millam, M. Klene, J. E. Knox, J. B. Cross, V. Bakken, C. Adamo, J. Jaramillo, R. Gomperts, R. E. Stratmann, O. Yazyev, A. J. Austin, R. Cammi, C. Pomelli, J. W. Ochterski, R.-L. Martin, K. Morokuma, V.-G. Zakrzewski, G. A. Voth, P. Salvador, J.-J. Dannenberg, S. Dapprich, A.-D. Daniels, Ö. Farkas, J.-B. Foresman, J.-V. Ortiz, J. Cioslowski, and D.-J. Fox, Gaussian, Inc., Wallingford CT, **2009**.